Features of a simvastatin-loaded multi-layered co-electrospun barrier membrane for guided bone regeneration

DAN YU[1*], CHONGSHANG HUANG[1*], CHU JIANG[2] and HUIYONG ZHU[1]

[1]Department of Oral and Maxillofacial Surgery, The First Affiliated Hospital, Zhejiang University School of Medicine, Hangzhou, Zhejiang 310003; [2]Department of Stomatology, Jiangshan People's Hospital, Jiangshan, Zhejiang 324100, P.R. China

Received May 8, 2020; Accepted March 15, 2021

DOI: 10.3892/etm.2021.10145

Abstract. A novel tri-layer membrane consisting of polycaprolactone (PCL) fibrous sheets and structured nanofibers with a gelatin (Gt) shell and a simvastatin-containing PCL core (PCL-Gt/PCL-simvastatin membrane) was prepared. The soft external layer comprised of Gt/PCL-simvastatin, the external layer of PCL and the middle layer of both microfilaments, interwoven together. The membrane was designed to promote osteoinduction and act as a barrier against cells but not against water and molecules in order to promote guided bone regeneration. The structure of the membrane was characterized by scanning electronic microscopy. The *in vitro* release rates of simvastatin over 32 days were determined by high-performance liquid chromatography. For *in vitro* biological assays, bone marrow mesenchymal stem cells and human fibroblasts were cultured on the different surfaces of the membrane. Cell adhesion, proliferation, distribution, and differentiation were examined. For *in vivo* testing, cranial defects were created in rabbits to assess the amount of new bone formed for each membrane. The results revealed that membranes with multi-layered structures showed good cell viability and effective osteoinductive and barrier properties. These results suggest that the novel multi-layered PCL-Gt/PCL-simvastatin membranes have great potential for bone tissue engineering.

Introduction

In bone tissue engineering, the use of composite carriers that encapsulate bioactive components is a key strategy for drug delivery. Carriers may contain drugs, small molecules or even nanomaterials (1,2). Electrospun nanofibers are effective biocompatible drug carriers because of their ability to repair bone tissue. These fibers can deliver significant amounts of therapeutics and have, therefore, attracted attention as potential drug delivering scaffolding materials (3,4). In addition, nanofibers are highly porous, providing an artificial milieu that is structurally comparable to the naturally occurring extracellular matrix (ECM) (1,5). As such, electrospun nanofibers are frequently utilized in tissue engineering (1,6,7). Electrospinning can also produce nanofibers with high bioactivity. These are based on natural polymers, including gelatin (Gt), chitosan and hyaluronic acid, and synthetic polymers, including poly-D, L-lactide-coglycolide (PLGA), polycaprolactone (PCL) and polyurethane. These polymers are all highly biocompatible and biodegradable (5).

Guided bone regeneration (GBR) has been demonstrated to be effective in periodontal therapy (8) and is an important strategy in bone tissue engineering (9). In GBR, the typical barrier membrane consists of two surfaces: The porous surface that faces the osseous bone defect, to guide bone formation, and the dense surface that faces the soft tissue, to prevent non-osteogenic cells (such as fibroblasts) from interfering with bone healing (10). Thus, the barrier membrane plays a crucial role in bone regeneration (8). In recent years, co-electrospinning has been used to generate hybrid nanofibers with specific features, such as its interconnected porous structures, broad surface areas and capability of delivering drugs (11-13). These nanofibers have the features of both naturally occurring and synthetic polymers, which improve their ability to induce bone tissue repair. Multi-layered scaffolds are also useful for vascular tissue engineering (14-16). The structural diversity of these scaffolds is more advantageous than homogeneous structures due to their enhanced mechanical features, biodegradability and biocompatibility (14,17,18). Unfortunately, complications such as delamination (poor biomechanics and operability) and difficulty in molding three-dimensional structures (compact structure that can impede cell migration) with many constituents have restricted the widespread development of multi-layered scaffolds (19,20).

Simvastatin, a cholesterol-lowering drug, can promote bone growth and this is hypothesized to be through stimulation of BMP-2 expression (21,22). Simvastatin has also been

Correspondence to: Dr Huiyong Zhu, Department of Oral and Maxillofacial Surgery, The First Affiliated Hospital, Zhejiang University School of Medicine, 79 Qingchun Road, Hangzhou, Zhejiang 310003, P.R. China
E-mail: zhuhuiyong@zju.edu.cn

*Contributed equally

Key words: co-electrospinning, guided bone regeneration, simvastatin, multi-layered, controlled release

successfully integrated into drug delivery vehicles consisting of a methylcellulose gel surrounded by a polylactic acid (PLA) membrane. Using this system, a single administration of 2.2 mg of simvastatin was demonstrated to induce bone growth *in vivo*, however, soft-tissue inflammation was observed (23).

In the present study, two multi-layered co-electrospun nanofibers membranes made of natural (Gt) and synthetic (PCL) polymers were designed. These membranes have both porous and dense layers to improve their osteogenic efficacy and barrier function. In addition, these membranes were loaded with simvastatin to promote bone growth (Fig. 1). These membranes were designed to promote osteoinduction and act as a barrier against cells but not against water and molecules in order to promote guided bone regeneration (GBR). The *in vitro* biological function of the membranes was then evaluated. In order to verify the osteogenic and barrier effects of the membranes, bone marrow mesenchymal stem cells (BMMSCs) and human fibroblasts were seeded on the surface of the porous and dense layers, respectively. The cell distribution on the different surfaces was observed using a confocal laser scanning microscope (CLSM). The osteogenic effects of simvastatin on critically-sized calvarial defects in rabbits were evaluated to assess the membrane's potential for GBR.

Materials and methods

Materials. PCL (85 kDa) and histopaque-1077 were obtained from Sigma-Aldrich (Merck KGaA). 2,2,2-trifluroroethanol (TFE) was obtained from the Weihai Newera Chemical Co., Ltd. Gelatin (Gt, 200 Bloom) was supplied by the Department of Polymer Science and Engineering, Zhejiang University (China). Simvastatin was purchased from BioSino Biotechnology & Science, Inc. 0.05% trypsin-5 Mm EDTA was from Biochrom GmbH (Merck KGaA). Human foreskin fibroblasts (HFFs-1) were obtained from the American Type Culture Collection. Culture media and other cell culture medium supplements were obtained from Thermo Fisher Scientific, Inc.

Preparation of the multilayered nanofibers. Simvastatin was dissolved in a PCL (20% w/w in TFE) solution to obtain a final concentration of 3.5%. Gt was dissolved in TFE to obtain a 12% solution. Coaxial electrospinning was conducted with reference to a previous study (24). The Gt/TFE solution was used to create the outer shell, while the PCL/TFE solution containing simvastatin was used to create the inner core. All feed rates were set at 1 ml/h. The spinning electrode and the collector were separated by 16 cm, with a voltage of 9-10 kV/cm. Collection was carried out over 3 h to obtain the Gt/PCL-simvastatin membrane. A single jet was used to electrospin the PCL mat on the Gt/PCL-simvastatin membrane. The spinning electrode and the collector were 17 cm apart, with a voltage of 11-12 kV/cm. The duration of electrospinning was 4 h, and the feed rate was 1 ml/h. Finally, a bi-layered PCL-Gt/PCL-simvastatin membrane (membrane A) was obtained. The layers were 100-150 μm thick.

The tri-layered PCL-Gt/PCL-simvastatin membrane (membrane B) was fabricated in a similar manner to membrane A. First, the coaxial Gt/PCL-simvastatin fibers were electrospun for 2 h, followed by the introduction of PCL nanofibers onto the coaxial membrane by simultaneous spinning using another electrode. The position of the spray nozzle for the PCL nanofibers was adjusted to ensure maximum overlap of the receiving area of the core-shell and PCL fibers. The two nanofibers were collected for 1.5 h, before coaxial electrospinning was stopped. The electrospinning of the PCL nanofibers was continued for 2 h. The structure of the multiple-layered nanofibrous membranes is shown in Fig. 1. The membranes were stored at room temperature.

Scaffold characterization. A scanning electron microscope (SEM; model no. JSM-5300; JEOL, Ltd.) was used to assess the surface and morphology of the nanofibers under x1,000 magnification. Image-Pro Plus v6.0 (Media Cybernetics, Inc.) was used to measure the average fiber diameter and pore size (n=100) of the materials. The samples used for SEM were subjected to vacuum drying and were sputter-coated with gold-palladium for 60 sec.

In order to evaluate nanofiber degradation, three membrane pieces were immersed in 10 ml phosphate-buffered saline (PBS, pH 7.2±0.1) and placed in a 37˚C water bath for 1 and 3 months, with PBS refreshed monthly. Sample degradation was examined by SEM observation.

The membranes were cut into squares (10x10 mm; n=3) and used to assess the *in vitro* release of simvastatin over one month. After sterilization using Cobalt-60 (2 h), the specimens were immersed in PBS (1 ml) and incubated at 37˚C under rotation (150 RPM). Supernatants were obtained daily and stored at -20˚C, with the addition of fresh PBS (1 ml). The amount of released simvastatin was assessed by high-performance liquid chromatography (HPLC), and the cumulative release of simvastatin was plotted.

Culture of bone marrow mesenchymal stem cells (BMMSCs). BMMSCs were isolated from iliac crest marrow aspirates of human donors (aged 20-25 years) with no known disease (n=4). Informed consent was obtained and signed by the donors and the study was approved by the Research Ethics Committee of The First Affiliated Hospital, College of Medicine, Zhejiang University (Hangzhou, China; Reference number 2013-273). The human samples were collected in the operating room of The First Affiliated Hospital of Zhejiang University School of Medicine between November 2014 and October 2020.

The isolation and culture procedure of BMMSCs were performed as described in our previous study (25). Histopaque-1077 density gradient centrifugation was used for BMMSC isolation. The collected mononuclear cells (MNCs) underwent PBS washes and resuspension in Dulbecco's modified Eagle's medium (DMEM) containing 10% fetal bovine serum (FBS) and 100 U/ml penicillin/streptomycin and were plated at a density of $2x10^6$ MNCs/cm^2. Incubation was carried out at 37˚C in a humidified environment containing 5% CO_2, and the medium was replenished at 3-4-day intervals. At 80% confluency, BMMSCs were passaged after trypsinization.

Seeding and culturing of cells on the membranes. BMMSCs at passage 3 were seeded on the coaxial surface of the membranes (10x10 mm) after sterilization (Cobalt-60, 2 h), placed in

Table I. Primer sequences of target and housekeeping genes that were utilized in the study.

Gene	Primer Sequence (5'-3')
Cbf-α1	F: TTCCAGACCAGCAGCACTC
	R: CAGCGTCAACACCATCATT
ON	F: CGAGCTGGATGAGAACAACA
	R: AAGTGGCAGGAAGAGTCGAA
ALP	F: GTCACTGCGGACCATTCC
	R: GGCTGCATACGCCATCAC
OCN	F: CAGCCACCGAGACACCATG
	R: CAGAGCGACACCCTAGACC
OPN	F: CAGTTGTCCCCACAGTAGACAC
	R: GTGATGTCCTCGTCTGTAGCATC
GAPDH	F: GGAGCG AGATCCCTCCAAAAT
	R: GGCTGTTGTCATACTTCTCATGG

F, forward; R, reverse; ON, osteonectin; ALP, alkaline phosphatase; OCN, osteocalcin; OPN, osteopontin; Cbf-α1, core-binding factor-α1.

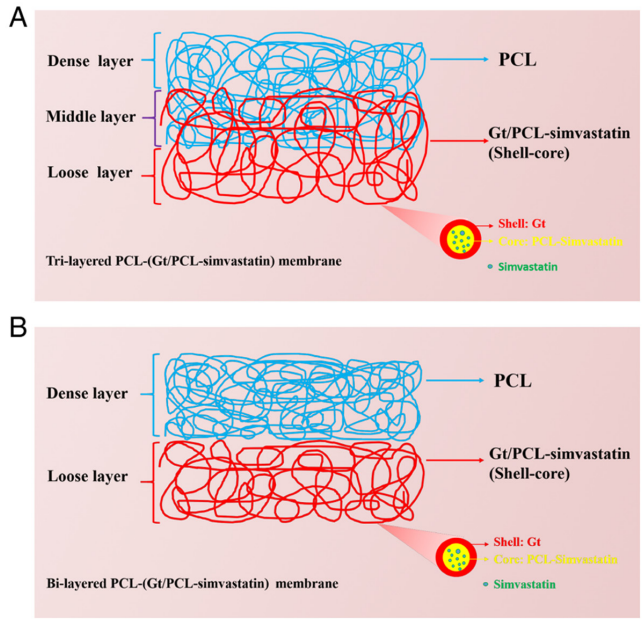

Figure 1. Schematic structure of the multi-layered membranes. (A) The bi-layered membrane consisted of a porous (co-axial Gt/PCL nanofibers loaded with simvastatin) and a dense (PCL nanofibers) layer. (B) The tri-layered membrane consisted of porous, middle and dense layers and was also loaded with simvastatin. The middle layer was obtained by interweaving Gt/PCL-simvastatin fibers and PCL fibers. Gt, gelatin; PCL, polycaprolactone.

a 24-well culture plate under pressure (glass column), and incubated overnight in a humid environment containing 5% CO_2 at 37˚C, as previously described (25,26). For seeding, cells at 5.4x10^6 cells/ml were added drop by drop onto the membrane, with approximately 3.2x10^5 cells per membrane. Third-passage HFFs-1 were added to the PCL surface of the membranes, as described above, at 5.4x10^6 cells/ml. Membrane A was used as the control group and membrane B as the experimental group. Constructs were incubated for 2.5-3 h to ensure cell adhesion to the membrane. Incubation was performed at 37˚C, as described above, with the medium refreshed at 3-4-day intervals. At defined time points, triplicates per seeding group were obtained for cell adhesion, distribution and differentiation assessment.

Cell morphology, proliferation, and distribution on membranes. To assess cell adhesion and morphology, cell-loaded membranes at 10, 30 and 60 min post-seeding were submitted to two PBS washes, glutaraldehyde fixation (2.5%; 2 h; 4˚C), and two additional PBS washes. Graded ethanol solutions (30, 50, 70, 80, 90, 95 and 100%) were used for dehydration, followed by sputter coating with gold and SEM analysis.

Cell proliferation was estimated with the Cell Counting Kit-8 (CCK-8; Dojindo Molecular Technologies, Inc.) after the cells were cultured on the membranes for 1, 3, 5 and 7 days. Cell proliferation was compared to cells seeded on Petri dishes as control. CCK-8 solution (10 μl) was added to each well (three wells for each group) and the cells were incubated at 37˚C for 4 h. Absorbance at 450 nm was determined using a microplate reader (Bio-Tek Instruments, Inc.).

For cell distribution assessment, PBS-washed cell-loaded membranes were incubated with 4',6-diamidino-2-phenylindole (DAPI; Invitrogen; Thermo Fisher Scientific, Inc.) for 30 min, washed, and further incubated in fresh medium for 1 h. These procedures were performed at 37˚C in a humidified 5% CO_2 atmosphere. Laser confocal scanning microscopy was performed and raw 3D images were analyzed using NIS-Elements Basic Research v3.0 (Nikon Instruments Inc.) for cell distribution.

Reverse transcription-quantitative PCR (RT-qPCR) for the determination of osteogenic gene expression. Total RNA from cell-membrane samples was obtained using the RNeasy micro kit (Qiagen GmbH). RNA amounts and purity were assessed on a Bio-Photometer (Eppendorf). First-strand cDNA (in 100-μl reaction volumes) synthesis was performed with a QuantiTect Reverse Transcription kit (Qiagen GmbH) based on 100 ng of total RNA, as recommended by the manufacturer (37˚C for 15 min and 85˚C for 5 sec). qPCR was carried out on an Applied Biosystems 7500 Real-Time PCR System (Life Technologies; Thermo Fisher Scientific, Inc.) with a QuantiTect SYBR Green PCR kit (Qiagen GmbH). Reactions contained 1 μl of cDNA, 4.5 μl of Real Master Mix/SYBR solution (Qiagen GmbH), 1 μl of each primer and 2.5 μl of RNase-free water. The early-stage osteogenic differentiation gene core-binding factor-α1 (Cbf-α1) (27,28) and alkaline phosphatase (ALP) (29), the middle-to-late stage osteogenic marker osteonectin (ON) (30), and the late stage markers osteocalcin (OCN) and osteopontin (OPN) (31) were assessed using glyceraldehyde-3-phosphate dehydrogenase (GAPDH) for normalization. Cells cultured without a membrane constituted the control group for assessing target gene expression. The primer sequences used are listed in Table I. Amplification was carried out for 40 cycles in a real-time PCR device, with a program consisting of HotstarTaq DNA polymerase activation (2 min, 95˚C), denaturation (15 sec, 95˚C) and annealing for 15 sec at 62˚C (ON, OCN, OPN), 63˚C (Cbf-α1) or 59˚C (GAPDH), with a final extension (20 sec, 68˚C). Cycle

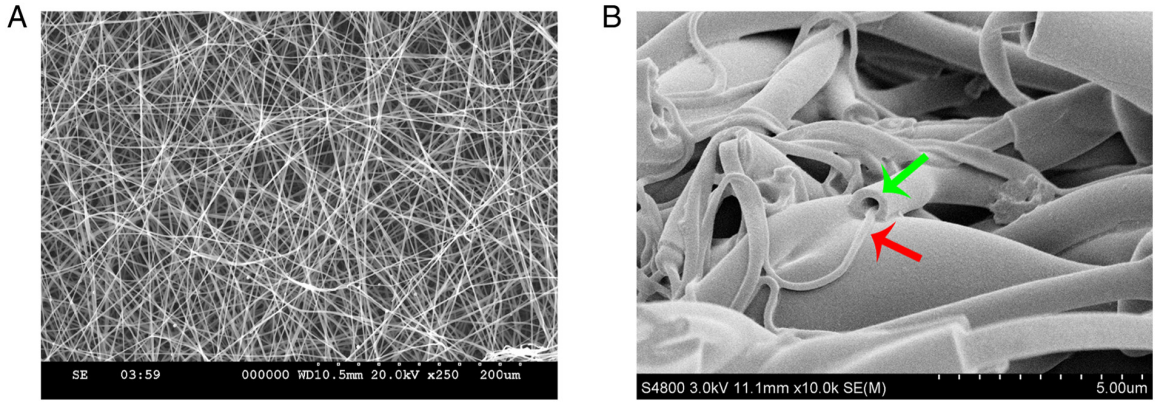

Figure 2. Morphology of the multi-layered PCL-Gt/PCL-simvastatin membrane was evaluated by SEM. (A) The structure of the membrane is interwoven with nanofibers, which are arranged randomly and have numerous holes of uneven size. (B) Co-axial nanofibers with a smooth surface consisted of core (PCL, red arrow) and shell (Gt, green arrow) structures. Gt, gelatin; PCL, polycaprolactone; SEM, scanning electron microscopy.

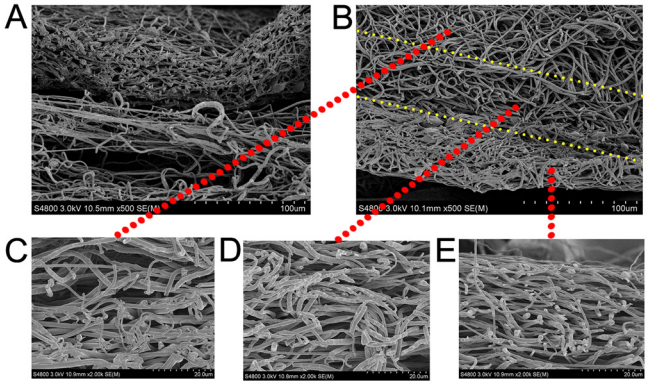

Figure 3. Structure of the membrane. (A) Obvious delamination was observed in membrane A, with a PCL mat on the upper layer and Gt/PCL-simvastatin membrane on the bottom. (B) A multi-layered structure was observed in membrane B. There was (C) a co-axial Gt/PCL-simvastatin nanofiber layer with smooth fibers and bigger pores, (D) a middle layer that consisted of two nanofibers and (E) a PCL nanofiber layer with more corrugations and small pores (from top to bottom). Gt, gelatin; PCL, polycaprolactone.

threshold (Ct) values and melting curves were assessed. The analysis was performed as described by Pfaffl (32).

Assessment of in vivo implants

Surgery. Critical-size defects were surgically created on the calvaria of 8-month-old New Zealand white rabbits (male, 2.0-2.5 kg; n=24) (21,31-38) purchased from the Laboratory Animal Center of Zhejiang Province. The rabbits were assigned to three groups: Control group (no membrane), group A (bi-layered PCL-Gt/PCL-simvastatin membrane) and group B (tri-layered PCL-Gt/PCL-simvastatin membrane). The Animal Experimental Ethical Committee of the First Affiliated Hospital, College of Medicine, Zhejiang University (Reference no. 2013-273) approved the protocols for animal experiments. The implantation procedures in these rabbits were performed under general anesthesia using fentanyl/fluanison (Hypnorm®, fentanyl citrate 0.315 mg/ml, fluanisone 10 mg/ml, Janssen Pharmaceuticals, Inc.; Johnson + Johnson; 0.3 ml/kg intramuscular) combined with an intravenous injection of 1 mg/kg diazepam. During surgery, full-thickness flaps were made to reveal the cranial bone, and critical size (15 mm) defects, as previously described (23,33-40), were generated with trephines under irrigation with chilled saline. For the membrane groups, the membranes were implanted and fixed onto the defects at this stage. A resorbable suture was used for closure of the soft tissues in layers. The rabbits underwent euthanasia with an overdose (100 mg/kg) of intravenous pentobarbital sodium at 4 or 12 weeks following implantation (n=4) and were assessed for bone regeneration.

Micro-computed tomography (μ-CT). At 4 or 12 weeks after implantation, the tissues surrounding the membranes were harvested and fixed in 10% formalin at room temperature for 24 h. Imaging was carried out on an animal micro-CT scanner (SCANCO Medical AG) in high-resolution scanning mode using 70 kV, 200 μA, a field of view of 15 mm and 34.4-μm resolution. Data analysis was performed with the micro-CT image analysis software (NRecon v.1.6.9; Bruker micro-CT; Bruker Corporation) to determine the mean new bone volume (BV), bone mineral density (BMD) and bone volume/total volume (BV/TV).

Histological analysis. Half of the samples underwent fixation with 10% formalin at room temperature for 24 h, decalcification, dehydration, paraffin embedding and hematoxylin and eosin (H&E) staining (26). The remaining half of the samples were fixed in 4% formalin (Formafix, Global Technologies Ltd.) at room temperature for 7 days and dehydrated for 14 days with increasing concentrations of alcohol (70, 80, 96 and 100%). Over a period of 28 days, the sections were block-embedded in polymethyl methacrylate (PMMA; Technovit® 7200 VLC; Kulzer GmbH), after which the samples were ground in the sagittal direction and sliced into 250-μm thick sections with a microtome (EXAKT Technologies, Inc.). The sections were further reduced to 15 μm, polished and stained with Van Gieson and toluidine blue, as described previously (41). Images were captured using an IX 70 light microscope (Olympus Corporation; magnification, x25). Three fields of view were observed for each section.

Statistical analysis. SPSS v11.5 (SPSS, Inc.) was used for the statistical analyses. Values are presented as the

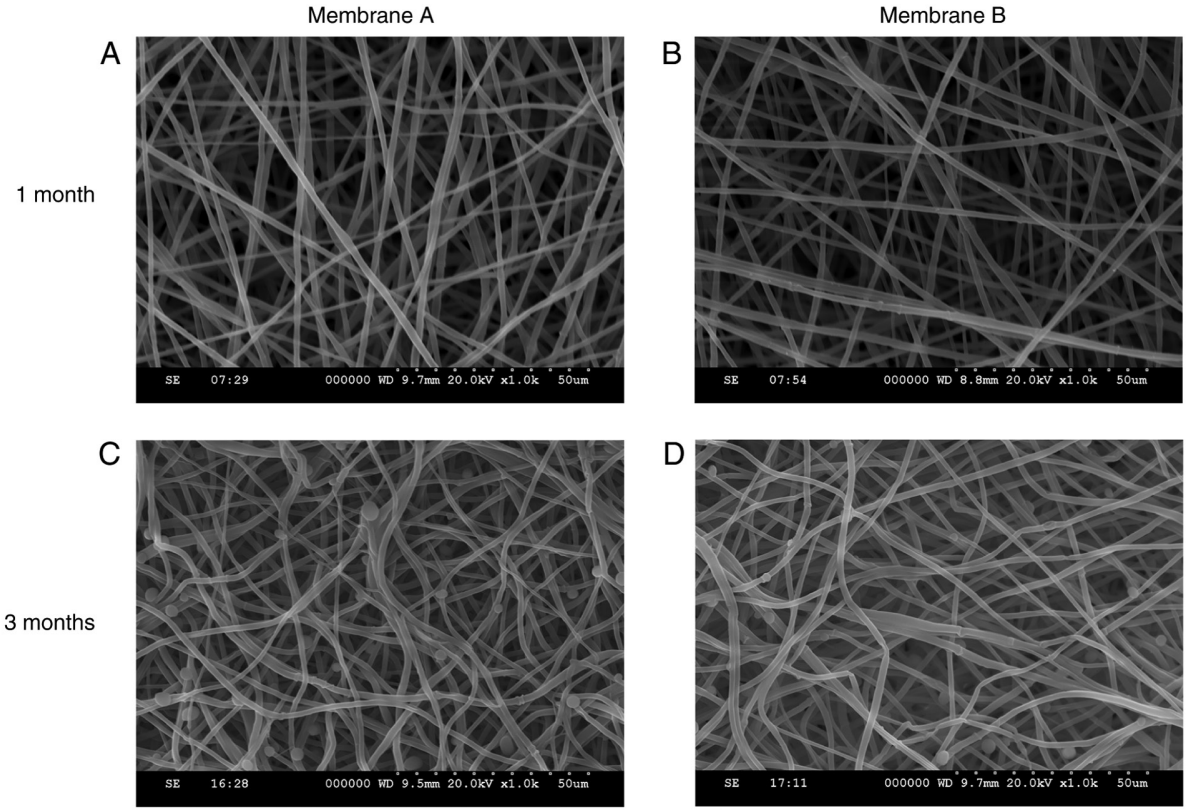

Figure 4. Scanning electron micrographs of different membranes after biodegradation for 1 and 3 months. (A) Membrane A after 1 month. (B) Membrane B after 1 month. After 3 months, the fibers of (C) membrane A and (D) membrane B became less distinct than the membranes after biodegradation for 1 month.

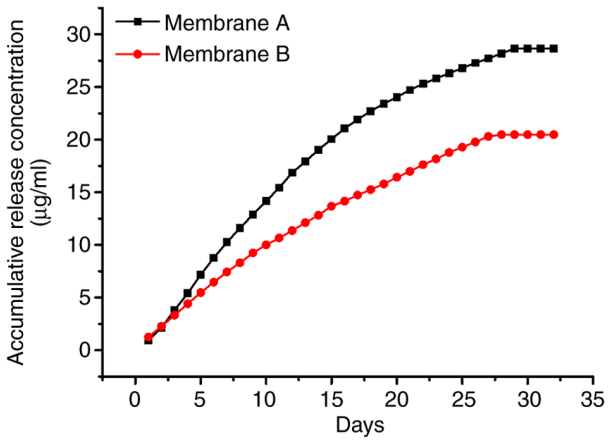

Figure 5. Simvastatin release profiles for the different structured membranes. The values are presented as the mean (n=3).

mean ± standard deviation (SD). Groups were compared by one-way analysis of variance (ANOVA) with Tukey's post hoc test/$P<0.05$ was considered to indicate statistical significance.

Results

Morphological and structural features. The preparation process of the tri-layered PCL-Gt/PCL-simvastatin membrane (membrane B) is shown in Fig. 1. The middle layer of membrane B was generated by the simultaneous spinning of uniaxial PCL and coaxial Gt/PCL-simvastatin nanofibers using two nozzles. As a control, the bi-layered PCL-(Gt/PCL-simvastatin) membrane (membrane A) was made with two separated fibrous mats by sequential electrospinning. As shown in Fig. 1A, the Gt/PCL-simvastatin and PCL nanofibers resulted in the porous and dense layers, respectively, while the middle layer of membrane B contained both types of fibers.

As indicated by the SEM images, electrospun nanofibers were smooth. This indicates that both PCL and Gt/PCL-simvastatin fibers could be generated under all flow rates and methods used (Fig. 2A). The two types of nanofibers had different morphologies. The pore sizes of the Gt/PCL-simvastatin nanofibers (porous layer) were 30.27±4.23 μm (membrane A) and 31.84±4.43 μm (membrane B), while the fiber diameters were 419.28±59.23 nm (membrane A) and 444.62±96.53 nm (membrane B). The pore sizes of the PCL nanofibers (dense layer) were 13.88±4.38 μm (membrane A) and 14.75±2.96 μm (membrane B), while the fiber diameters were 228.58±98.12 nm (membrane A) and 254.73± 0.68 nm (membrane B). Fig. 2B demonstrates the general structure of the Gt/PCL fibers. The shell was composed of the natural polymer Gt, and the core was composed of the synthetic polymer PCL containing simvastatin. Fig. 2B does not represent the final structure of the membrane, nor its evolution in time.

The structural details of the membranes are shown in Fig. 3. Obvious delamination appeared in membrane A with the PCL mat on the top and Gt/PCL-simvastatin membrane on the bottom (Fig. 3A), while no delamination was observed in membrane B (Fig. 3B). SEM images demonstrating the morphology in membrane B are also shown. The changes in structure and morphology in the different layers indicated a

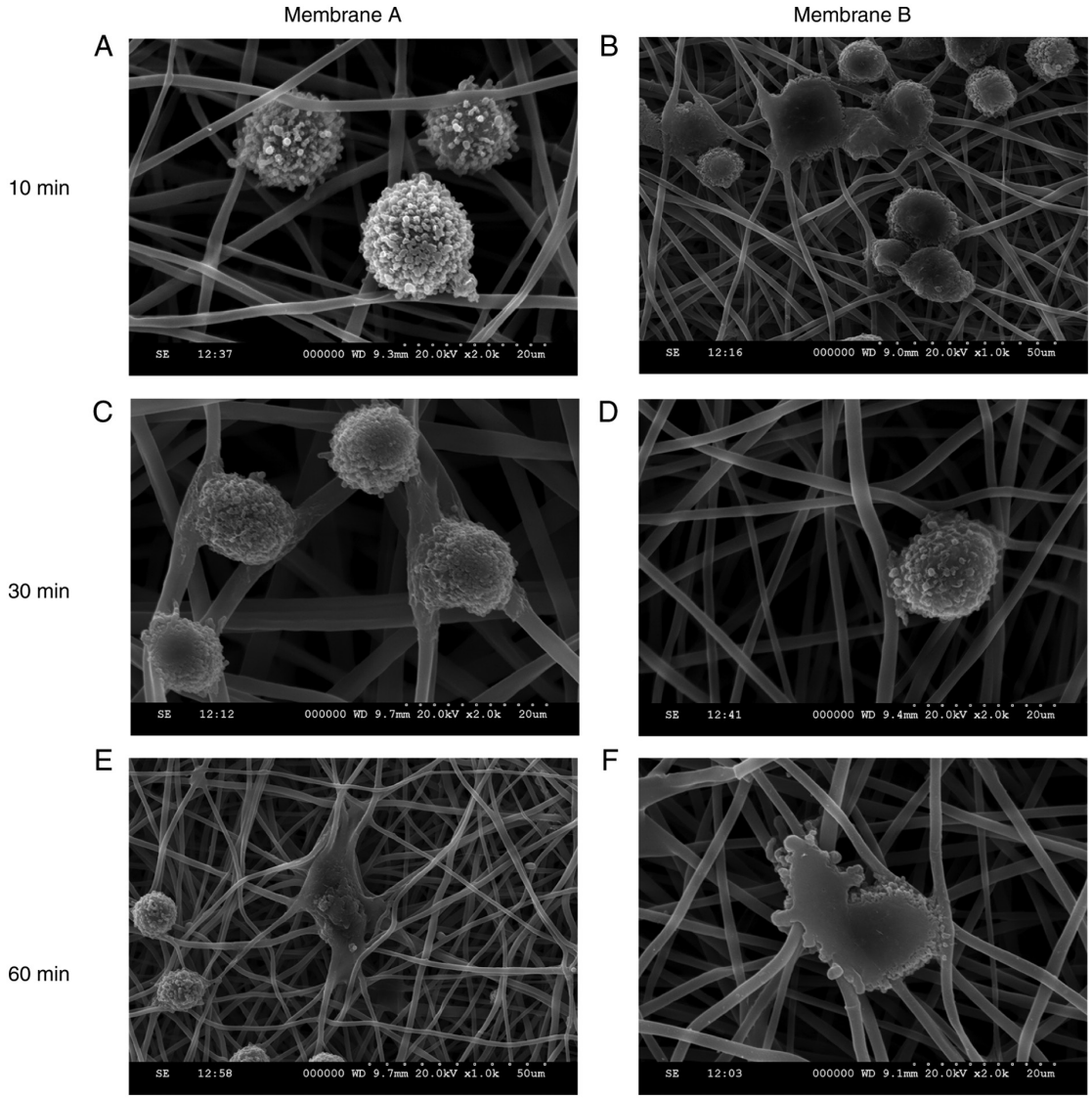

Figure 6. SEM micrographs showing the adhesion of BMMSCs to the porous surface of different membranes at early stages. After seeding on the membrane, the BMMSCs attached themselves to nanofibers. As time went by, the cells stretched out along the fiber processes on the membrane in all directions. Adhesion of cells to (A) membrane A and (B) membrane B after 10 min. Adhesion of cells to (C) membrane A and (D) membrane B after 30 min. Adhesion of cells to (E) membrane A and (F) membrane B after 60 min. SEM, scanning electron microscopy; BMMSCs, bone marrow mesenchymal stem cells.

distribution of multiple layers in the membrane. The upper layer was composed of coaxial electrospun fibers with a smooth surface (Fig. 3C). The layer between the dense and porous layers is the middle layer (Fig. 3D), while the lower PCL layer comprised greater corrugation nanofibers (Fig. 3E).

Biodegradability in vitro. SEM micrographs of the electrospun membranes during degradation are shown in Fig. 4. The porous layer of the nanofibrous membranes was morphologically intact during the first month. After 3 months, the coaxial nanofibers were partially dissolved, but the overall integrity of the fiber structure was maintained.

Simvastatin release from the electrospun fibers. The release profile of simvastatin from the core-shell structured fibers is shown in Fig. 5. Samples for assessing simvastatin release into the solution were obtained every day for 32 days, and the total simvastatin amounts were evaluated by HPLC. Approximately

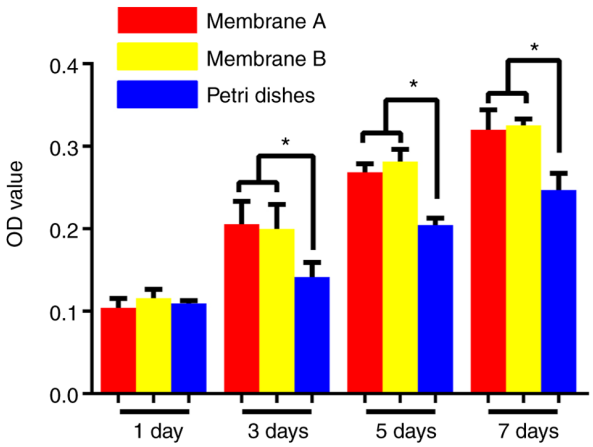

Figure 7. Cell proliferation of BMMSCs on membrane A, membrane B and Petri dishes (n=3). The results indicated that the cell proliferation rates on the membranes within 7 days were significantly higher than that on the Petri dishes but that there were no significant differences between the two membranes. BMMSCs, bone marrow mesenchymal stem cells. *P<0.05.

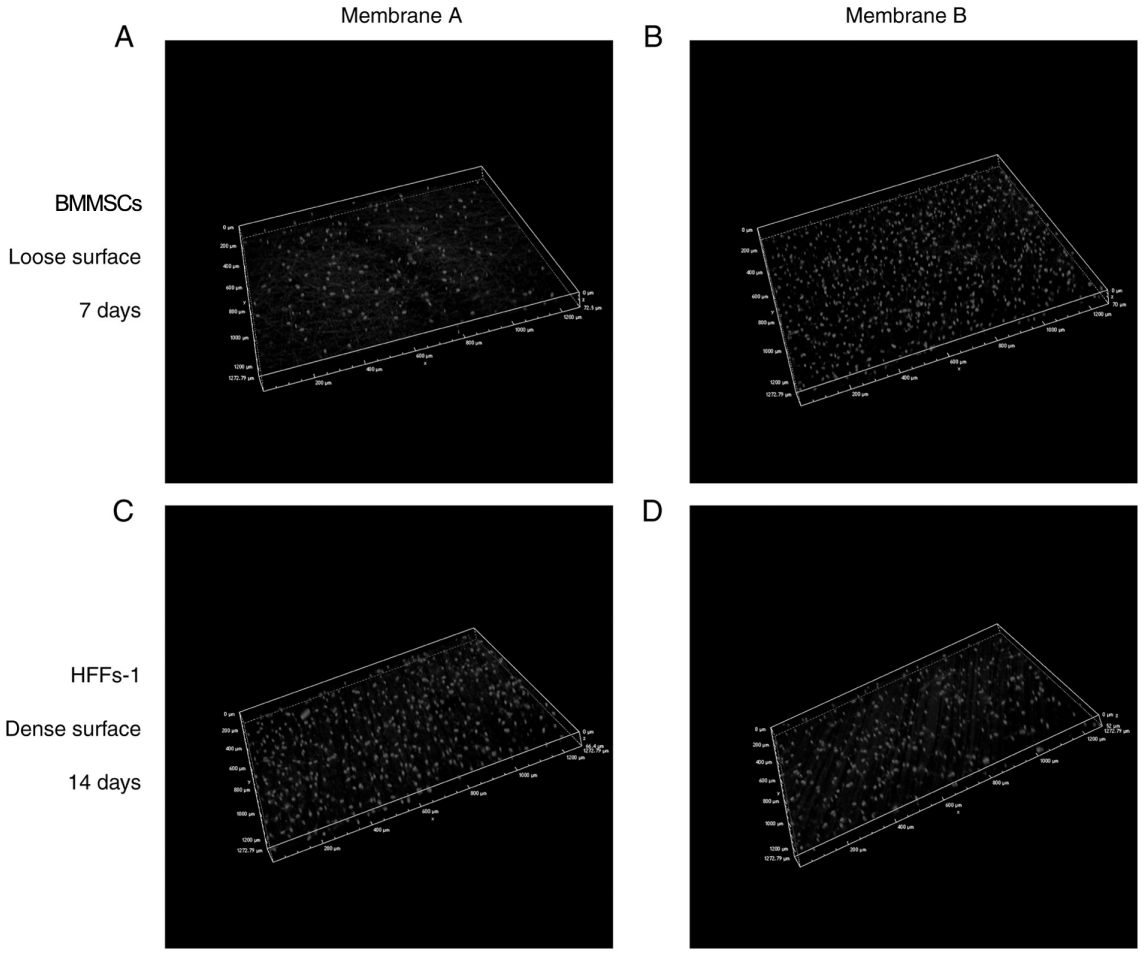

Figure 8. Confocal images of cells on different membranes after 7 and 14 days. The BMMSCs penetrated as deeply as 70 μm on the coaxial surface after 7 days on (A) membrane A and (B) membrane B, while HFFs on the PCL surface penetrated as deeply as 60 μm after 14 days on (C) membrane A and (D) membrane B. BMMSCs, bone marrow mesenchymal stem cells; HFF, human foreskin fibroblasts; PCL, polycaprolactone.

28.66 μg of simvastatin was released per membrane within the first 25 days. The cumulative release of simvastatin was linearly correlated with the incubation time at the early stage (about 15 days) and approached a plateau after 25 days.

Adhesion of BMMSCs to electrospun membranes. The adhesion of BMMSCs to the porous layer of the membranes is shown in Fig. 6. BMMSC adhesion was highly prominent at 10 min post-seeding. The cells stretched out along the fiber processes on the membrane in all directions, particularly at 60 min after seeding. No obvious differences were found between membranes A and B.

Cell proliferation on the membranes. The cell proliferative activity on the membranes was evaluated over 7 days (Fig. 7). Compared to the control group, the numbers of BMMSCs from the membrane groups were significantly higher than the numbers in the control group throughout the 7 days ($P<0.05$). However, there were no significant differences between the two membranes ($P>0.05$).

Cell distribution on the electrospun fibers. Confocal images showing cells on the fibers after culturing for 7 and 14 days are shown in Fig. 8. At 7 days, the porous surface of the membrane was covered by a continuous and structured MSC monolayer. The dense surface was covered by HFFs-1 at 14 days. The 3D image shows that the MSCs seeded on the porous surface of the membrane penetrated as deeply as 70 μm after 7 days, while HFFs-1 seeded on the dense surface of membrane penetrated as deeply as 60 μm after 14 days, indicating that the dense layer could act as an effective barrier to prevent cell invasion. No cells were observed to cross the membranes completely.

Osteogenic gene expression in BMMSCs on the fibers. While continuously co-culturing the MSC-membrane composite, osteogenic gene expression levels were comparable in groups A and B after 1, 7, 14 or 21 days (all $P>0.05$; Fig. 9), with peaks at 7 days. An exception was Cbf-α1 gene expression in MSCs grown on tri-layered PCL-Gt/PCL-simvastatin fibers, which was significantly increased at 7 days ($P<0.05$). ALP was also higher in membrane B than in membrane A at 7 days ($P<0.05$), while OCN was higher in membrane B at 21 days ($P<0.05$). There were no differences in OPN expression between the two membranes ($P>0.05$).

In vivo implantation. To assess the osteogenic defect of nanofibers *in vivo*, 15-mm complete calvarial defects were generated in rabbits. During the experiment, no necrosis was observed in the animals.

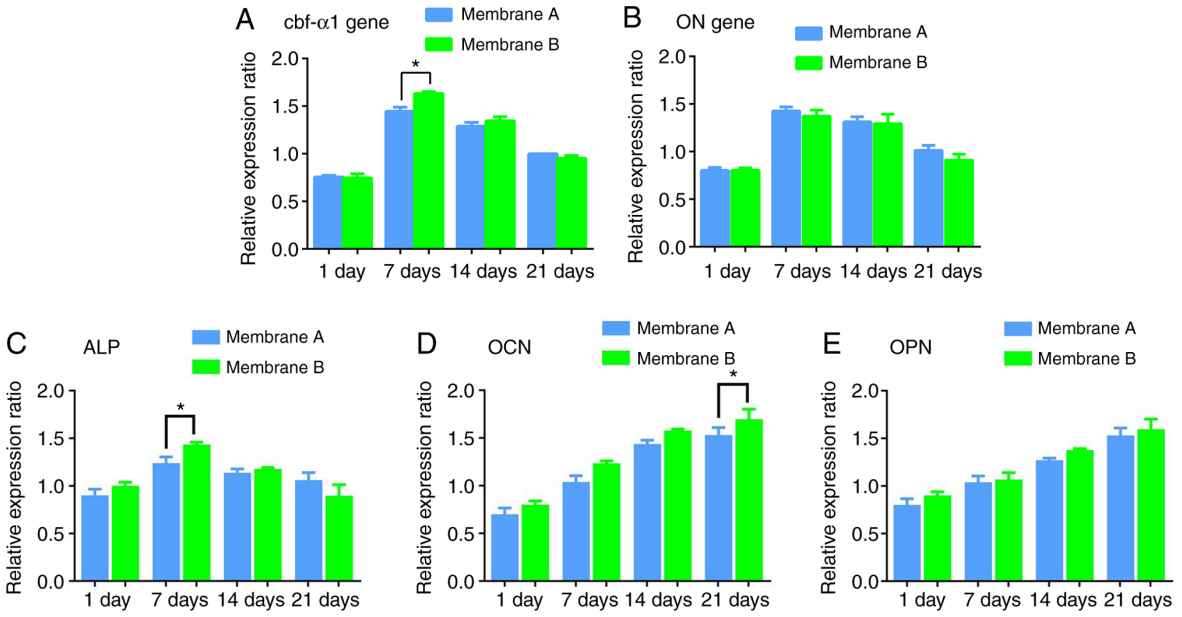

Figure 9. RT-qPCR analysis of the relative expression ratio of osteogenic genes in BMMSCs cultured on membrane A or B over 21 days. The target gene expression levels were calculated as a relative ratio to the house-keeping gene GAPDH. (A) Cbf-α1 gene expression. (B) ON gene expression. (C) ALP gene expression. (D) OCN gene expression. (E) OPN gene expression. Data are presented as the mean ± SD; n=3; *P<0.05. BMMSCs, bone marrow mesenchymal stem cells; Cbf-α1, core binding factor-α1; ON, osteonectin; ALP, alkaline phosphatase; OCN, osteocalcin; OPN, osteopontin.

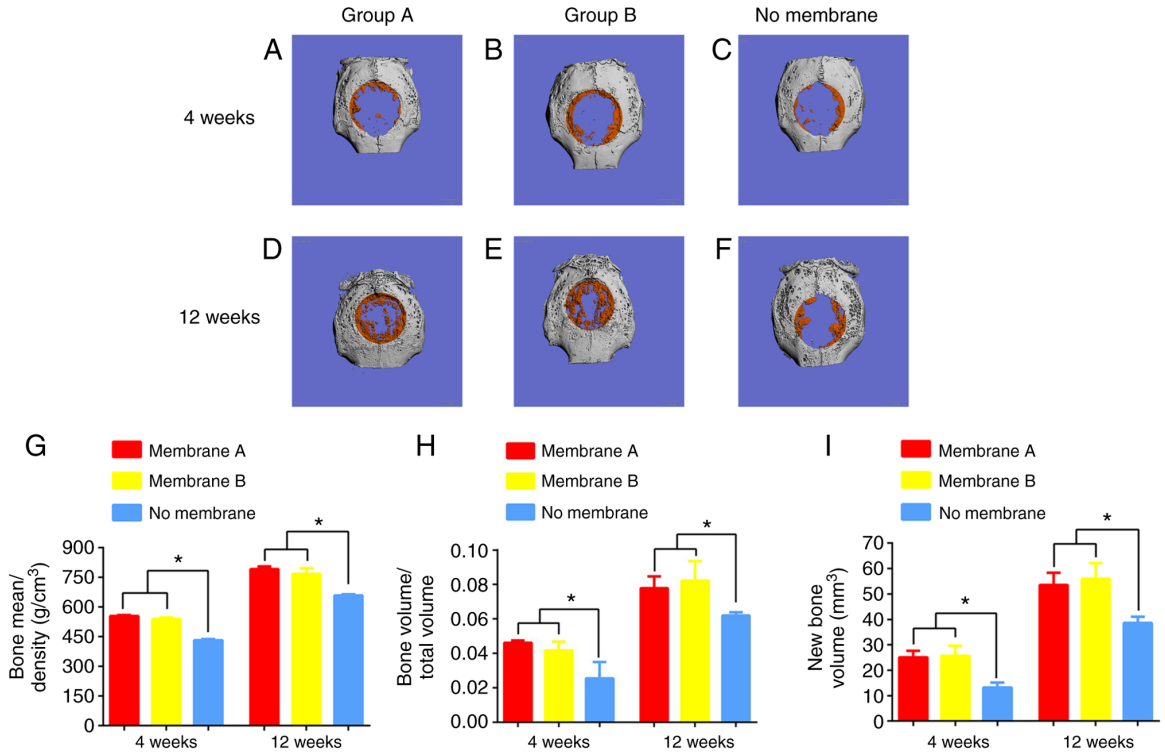

Figure 10. Micro-CT results of surgical defects treated with membranes A or B, or a no membrane (control group) at 4 and 12 weeks. Osteogenesis effects were seen in (A) group A and (B) group B in repair of the defect in comparison to (C) the control at 4 weeks. A greater extent of defect repair was also seen in (D) group A and (E) group B in repair of the defect in comparison to (F) the control at 12 weeks. There were more blue areas in the control group and more orange areas in groups A and B, where blue represents fibrous tissue, and orange represents new mineralized bone. At 12 weeks, the greatest extent of repair appeared in group B, and the defect region was mainly covered by orange. (G) BMD (mg/mm^3), (H) BV/TV (%) and (I) BV (mm^3) within the defects were calculated. BV, BMD, and BV/TV of groups A and B were significantly higher than in the control group at both 4 and 12 weeks. Data are presented as the mean ± SD; n=4; *P<0.05. BMD, bone mineral density; BV/TV, bone volume/total volume; new bone volume.

Micro-CT analysis. Bone formation was increased in the nanofiber groups compared with the control group at 4 and 12 weeks (Fig. 10A-F). Quantitation of μ-CT imaging data was carried out by assessing BV, BMD and BV/TV of the defects (Fig. 10G-I).

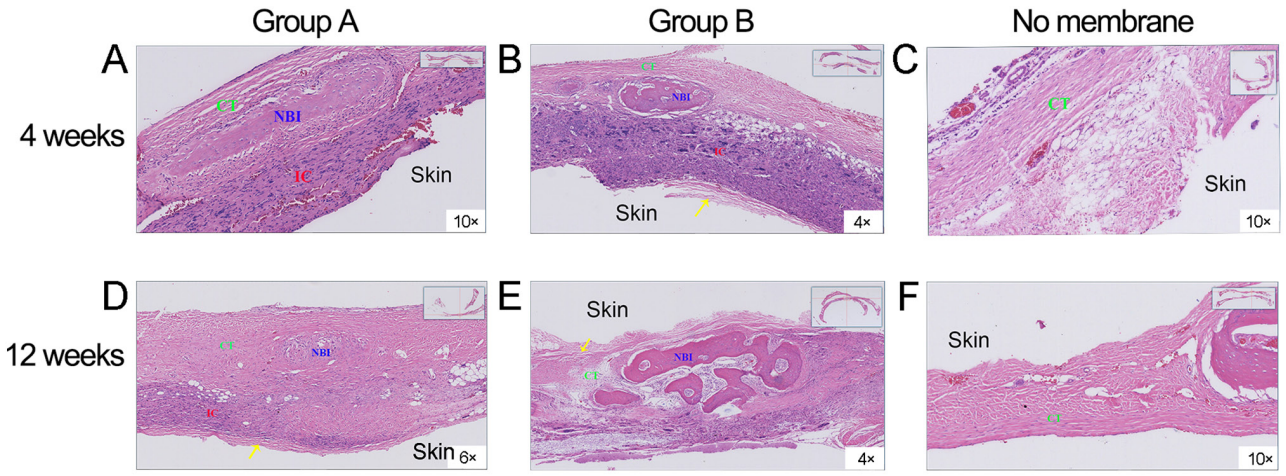

Figure 11. Histological study of transverse bone defect sections at 4 and 12 weeks after surgery. At 4 weeks, new bone generation was observed in (A) group A and (B) group B, while only soft tissues and limited new bone were observed in (C) controls. At 12 weeks, in comparison with (D) group A new bone area was markedly elevated in group B (E) Bone area was also elevated in comparison with (F) the control. Over time, residual membrane materials (yellow arrow) were observed in both membrane groups. The whole sections at low (x5) magnification are shown in small inserts in the upper right corner of each panel. CT, connective tissue; MB, mineralized bone matrix; NBI, new bone island; IC, inflammatory cells.

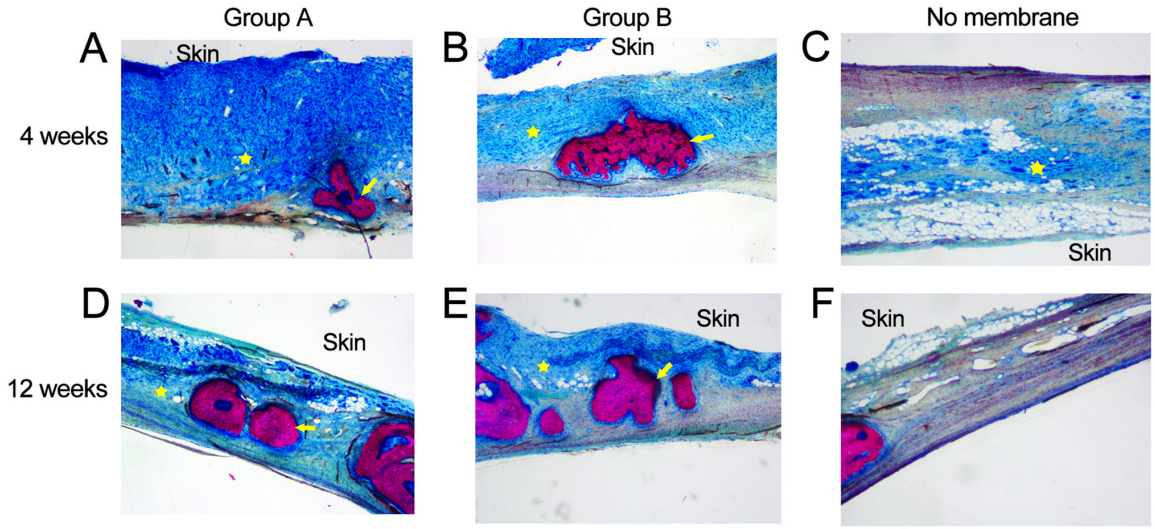

Figure 12. Van Gieson and toluidine blue staining of transverse bone defect sections at 4 and 12 weeks after surgery are consistent with H&E staining. New bone formation in (A) group A and (B) group B after 4 weeks occurred to a greater extent than in (C) the control group. In the control group only a large amount of connective tissue was observed. Similar results were observed at 12 weeks in (D) group A and (E) group B in comparison to (F) the control. Furthermore, compared with group B, there was more fibro-adipose tissue filling in the defect in group A and Group B had a narrower fibro-adipose tissue band. H&E, hematoxylin and eosin; Star, fibro-adipose tissue; arrow, mineralized bone matrix (x25).

Defects treated with membrane B showed healing with BV, BMD and BV/TV of 25.13±2.50 mm^3, 539.74±8.38 mg/mm^3 and 4.17±0.51%, respectively, at 4 weeks following implantation. New bone formation was similar in groups A and B and almost inexistent in the control group. At 12 weeks, new bone was found in the three groups. In comparison with controls, group B had markedly increased healing, with BV, BMD and BV/TV of 56.05±60.15 mm^3, 767.83±29.10 mg/mm^3 and 8.22±1.17%. In group B, bone formation covered most of the defects. By contrast, healing was only observed in the center or at the edges in controls. These findings demonstrated that the released simvastatin had *in vivo* activity.

Histological properties. Using eosin ethanol staining, new bone generation was observed in groups A and B at 4 weeks after surgery, whereas in the control group, only soft tissues and limited new bone were observed (Fig. 11). At 12 weeks, the new bone area was markedly elevated in group B in comparison with the two other groups. The control group only showed minimal fibrous-connective tissue. At the initial stage (4 weeks) of bone healing, an overt immunologic response with inflammatory signs were recorded. At 12 weeks, there were slight inflammatory signs in both membrane groups, indicating that the membranes were gradually degraded. Over time, residual membrane materials were observed in both membrane groups.

The results of Van Gieson and toluidine blue stain were consistent with the H&E staining results (Fig. 12). New bone formation in groups A and B occurred to a greater extent than in the control group at 4 and 12 weeks. In the control group, only a large amount of connective tissue was observed.

Discussion

Our previous studies demonstrated that the diameter of electrospinning nanofibers could be affected by flow rate and receiving distance (42,43). The parameters for the present study were optimized during our earlier studies (42,43). SEM revealed that the membranes were nano-scaled and that the co-axial electrospun Gt/PCL-simvastatin fibers had a distinct core-shell structure. Using a sequential quantity gradient co-electrospinning approach, PCL markedly improved the mechanical features of the nanofibers. The membrane structure was similar to that of the ECM, and the pore size of the PCL surface was significantly smaller than that of the coaxial surface. The present study demonstrated that the designed membrane had good morphological, physico-chemical and mechanical features that enable it to serve as a barrier membrane. Cross-sectional images of membrane B showed that the Gt/PCL-simvastatin and PCL nanofibers were well-mixed and integrated between the membrane layers. By contrast, membrane A was observed to have two layers without connection and could be easily separated.

An ideal drug delivery system should supply effective product amounts, avoid systemic undesired reactions, and convey products into target areas at fixed rates (44). The generation of a distinct boundary could be theoretically assessed (45,46). Studies by both our group (25) and others (47) have indicated that coaxial electrospinning can achieve effective product loading as well as continuous and controlled local drug delivery. In the present study, simvastatin was embedded in the core (PCL) of a coaxial structure. The mechanism of simvastatin release at a controlled rate can be explained by diffusion and polymer degradation (48,49). Simvastatin is first released by diffusion onto the fiber's surface. Subsequently, when the membrane is incubated with the medium, the small pores on the shell (Gt) of the fibers undergo gradual polymer degradation. This allows the slow and constant release of the drug through the pores. Both membranes in the present study demonstrated constant and continuous drug release, with membrane B demonstrating a more controlled drug release, due to its gradient structure.

Implantable materials should undergo *in vivo* degradation at a controlled rate to maintain and provide space for new bone formation (50). Material degeneration speed is critical in tissue engineering (51-54). If the membrane is degraded too fast, cell proliferation may be hampered, with insufficient secretion of the new matrix (51). Conversely, if degradation is too slow, residual materials could adversely affect new bone's homogeneity and function (55). Furthermore, the optimal time for degradation of materials in the skull or maxillofacial bones is 3-6 months, whereas the scaffold used in spinal fusion should be degraded after 9 months or longer (50). In the present study, an artificial synthetic material (PCL) was used to provide controlled release kinetics (47) and an appropriate degradation rate. The results of degradation testing *in vitro* suggested that the fiber surface became increasingly rough within 3 months, consistent with the optimal time of 3-6 months. Nevertheless, the complete degradation time of PCL is about 2 years, and future studies should examine for how long a PCL-based membrane retains its support and barriers effects. H&E staining also suggested that new bone islands and osteoid tissue had replaced the degraded membrane material at this time point. Furthermore, the timing coincides well with the release of simvastatin.

Electrospun nanofibers have high surface-to-volume ratios and are potential ECM substitutes that improve cell attachment (56,57). Simultaneously, high porosity confers optimal permeability for nutrient and gas exchange in the newly formed tissue (58). SEM of BMMSCs seeded membranes showed that cells were firmly attached to fibers, with cytoplasmic processes spreading throughout. This suggests that such membranes are an optimal scaffold for cell attachment. CCK-8 testing revealed that the membranes could promote cell adhesion and proliferation, with no cytotoxicity *in vitro*. The confocal microscopy results established that MSCs proliferated on the coaxial fibrous surface and the superficial layer of the internal part of the membrane. HFFs-1 with poorer adhesion and more superficial invasive depth also showed an excellent barrier function in membrane B. The same results were obtained from histological assessment of *in vivo* samples, with group B showing less fibrous tissue in the defect lending itself to ideal barrier function.

In order to assess the clinical usefulness of membrane B, a critical-sized defect in rabbit calvaria was created, based on previous studies (23,33-40). Micro-CT revealed an elevated BV/TV ratio, suggesting new bone generation, for both membrane groups compared with controls. Both membrane groups showed comparable values. *In vivo* histological data demonstrated that both membranes enhanced bone regeneration in comparison with controls. Meanwhile, *in vitro* testing of osteoinduction of simvastatin released from the membrane fibers revealed that osteogenic genes were upregulated in culture. Thus, simvastatin released from the membrane increases new bone generation and accelerates bone healing in the calvarial-defect model, but osteoinductive effects were comparable in both membrane groups.

The present study demonstrated that a novel multi-layered PCL-Gt/PCL-simvastatin membrane promoted osteogenesis in cultured BMMSCs and repaired bone defects in rabbits. As the sole bioactive agent, simvastatin could be successfully delivered and in a controlled manner. The role of multi-layered structured membranes in GBR technology remains unclear. These results suggest that the novel gradient nanofibrous membrane could be a candidate for an ideal barrier membrane, which is the primary end goal for current GBR technologies.

Inflammation could be seen in the specimens from the rabbits that received the membranes. Gelatin and PCL are widely-used polymers in the field of tissue engineering and are highly biocompatible and biodegradable (5). However, though simvastatin has been shown to induce bone growth *in vivo*, pronounced soft-tissue inflammation was observed (23). It can be hypothesized that this inflammation is the result of simvastatin, which was suggested by a previous study (59). Why simvastatin induces inflammation and how it might participate in the osteogenesis process remain to be examined.

The barrier membrane developed in this study is a guide for tissue regeneration. It has a loose surface and a dense surface. The loose surface faces the bone tissue to facilitate the crawling of bone cells or stem cells and guide bone tissue regeneration. The dense surface has a small pore size to prevent fibrosis. Since the regenerative cells invade the bone defect area while

the fibrotic cells invade from the connective tissues, the stem cells were inoculated on the loose surface and fibroblasts on the dense surface to observe the barrier function of the barrier membrane and guide the regeneration ability of totipotent stem cells. The differential impact of different cell types will have to be examined in a future study.

There are several limitations to this study. Multilayered membranes without simvastatin as controls were not included. Indeed, the main research focus of this article was on the structural innovation of the barrier membrane, rather than the bone-promoting function of simvastatin, which is relatively well-known (21,22). In addition, it has previously been shown that coaxial electrospinning can achieve effective product loading as well as continuous and controlled local drug delivery (26). The present study demonstrates the potential application of novel multilayered electrospun membranes for GBR with simvastatin in the treatment of bone regeneration.

The characteristics of cell donor may influence the results, however all donors in this study were 20-25 years of age and healthy, and the effect of age difference on BMMSCs should be minimal (60-62). In a published Master's degree thesis (entitled Osteogenic ability and differential gene expression profile of human bone marrow mesenchymal stem cells of different ages), BMMSCs from the fetal group (20-24 weeks of age), youth group (16-30 years), and elderly group (60+ years) showed consistent characteristics within their respective groups, but the osteogenic properties clearly decreased with age (63). In addition, the cell growth rate of donors over 50 years old was significantly lower than that of young donors. Furthermore, Choudhery *et al* (64) demonstrated that the BMSC markers do not change with age, but that the number of cells per gram, colony-forming units and the number of cells doubled per unit time decreases with the increase of the age of mesenchymal stem cells and donors. Fosset *et al* (65) also suggested that there is no age-related change in the expression of cell surface markers, however, Stolzing *et al* (66) reported that the expression levels of the MSC cell surface markers CD90, CD105 and stro1 decrease and CD44 increase, and that the differentiation potential is also different with age. In addition, Aksoy *et al* (67) suggested that various surface markers of MSCs are expressed at different ages, but compared with older donor cells, MSCs isolated from younger human donors have a higher cell metabolic activity and proliferation rate. Therefore, including cells from a single age group should minimize the variability due to age, however, some interindividual variability might remain.

Limits in image resolution and difficulties in accurately determining tissue regions may present a potential limitation of the present study. The applicability and clinical safety of the present study remain to be assessed in future studies, including more appropriate controls and intravital microscopy. Finally, the systemic concentrations of simvastatin were not determined, and it is unknown whether simvastatin can be released into the peripheral circulation and whether it could exert systemic effects that could influence bone regeneration, either directly or indirectly. This will have to be addressed in future studies.

In conclusion, a novel multi-layered PCL-Gt/PCL-simvastatin membrane was successfully established by coaxial electrospinning. This membrane is suitable for use in GBR. The membrane was able to deliver simvastatin continuously and promoted new bone formation without overt cytotoxic effects. This new coaxial electrospinning method might provide new means for fabricating membranes with both multi-layered structure and osteoinductive ability.

Acknowledgements

We are grateful to Dr. Zhengjian Chen at the Department of Polymer Science and Engineering, Zhejiang University and Prof. Jindan Wu at the MOE Key Laboratory of Advanced Textile Materials & Manufacturing Technology, Zhejiang Sci-Tech University for their help with the synthesis of the membranes used in this study.

Funding

The present study was funded by grants from the Medical and Health Major Science and Technology Plan of Zhejiang Province, China (grant no. wsk2014-2-008), the National Natural Science Foundation of China (grant no. 31570989), the Natural Science Foundation of Zhejiang Province of China (grant no. LY15H140002), the Young Talents Project of Zhejiang Provincial Health Department, China (grant no. 2019RC151) and Zhejiang Province Welfare Technology Research Project, China (grant no. LGF20H140007).

Availability of data and materials

The datasets used and/or analyzed during the current study are available from the corresponding author on reasonable request.

Authors' contributions

DY and CH characterized the morphology of the nanofibers and their release of simvastatin, assessed their biological function *in vitro*, analyzed and interpreted the data and was a major contributor to writing the manuscript. CH and HZ performed the histological examination *in vivo*. CJ and DY analyzed and interpreted the data. HZ was responsible for conceptualization, project administration, article review and quality control. DY, CH, CJ and HZ confirmed the authenticity of all raw data. All authors read and approved the final manuscript.

Ethics approval and consent to participate

The Animal Experimental Ethical Committee of the First Affiliated Hospital, College of Medicine, Zhejiang University (Reference no. 2013-273) approved the protocols for animal experiments. Informed consent was obtained and signed by the BMMSC donors and the human cell study was approved by the Research Ethics Committee of the First Affiliated Hospital, College of Medicine, Zhejiang University (Hangzhou, China; Reference number 2013-273).

Patient consent for publication

Not applicable.

Competing interests

The authors declare that they have no competing interests.

References

1. Rezvani Z, Venugopal JR, Urbanska AM, Mills DK, Ramakrishna S and Mozafari M: A bird's eye view on the use of electrospun nanofibrous scaffolds for bone tissue engineering: Current state-of-the-art, emerging directions and future trends. Nanomedicine 12: 2181-2200, 2016.
2. Yang G, Li X, He Y, Ma J, Ni G and Zhou S: From nano to micro to macro: Electrospun hierarchically structured polymeric fibers for biomedical applications. Prog Polymer Sci 81: 80-113, 2018.
3. Jang JH, Castano O and Kim HW: Electrospun materials as potential platforms for bone tissue engineering. Adv Drug Deliv Rev 61: 1065-1083, 2009.
4. Holzwarth JM and Ma PX: Biomimetic nanofibrous scaffolds for bone tissue engineering. Biomaterials 32: 9622-9629, 2011.
5. Mata A, Geng Y, Henrikson KJ, Aparicio C, Stock SR, Satcher RL and Stupp SI: Bone regeneration mediated by biomimetic mineralization of a nanofiber matrix. Biomaterials 31: 6004-6012, 2010.
6. Li C, Vepari C, Jin HJ, Kim HJ and Kaplan DL: Electrospun silk-BMP-2 scaffolds for bone tissue engineering. Biomaterials 27: 3115-3124, 2006.
7. Sharifi F, Atyabi SM, Irani S and Bakhshi H: Bone morphogenic protein-2 immobilization by cold atmospheric plasma to enhance the osteoinductivity of carboxymethyl chitosan-based nanofibers. Carbohydr Polym 231: 115681, 2020.
8. Kostopoulos L and Karring T: Augmentation of the rat mandible using guided tissue regeneration. Clin Oral Implants Res 5: 75-82, 1994.
9. Sedghi R, Shaabani A and Sayyari N: Electrospun triazole-based chitosan nanofibers as a novel scaffolds for bone tissue repair and regeneration. Carbohydr Polym 230: 115707, 2020.
10. Elgali I, Turri A, Xia W, Norlindh B, Johansson A, Dahlin C, Thomsen P and Omar O: Guided bone regeneration using resorbable membrane and different bone substitutes: Early histological and molecular events. Acta Biomater 29: 409-423, 2016.
11. Samavedi S, Olsen Horton C, Guelcher SA, Goldstein AS and Whittington AR: Fabrication of a model continuously graded co-electrospun mesh for regeneration of the ligament-bone interface. Acta Biomater 7: 4131-4138, 2011.
12. Dalgic AD, Atila D, Karatas A, Tezcaner A and Keskin D: Diatom shell incorporated PHBV/PCL-pullulan co-electrospun scaffold for bone tissue engineering. Mater Sci Eng C Mater Biol Appl 100: 735-746, 2019.
13. Wang Y, Cui W, Zhao X, Wen S, Sun Y, Han J and Zhang H: Bone remodeling-inspired dual delivery electrospun nanofibers for promoting bone regeneration. Nanoscale 11: 60-71, 2018.
14. Liu S, Dong C, Lu G, Lu Q, Li Z, Kaplan DL and Zhu H: Bilayered vascular grafts based on silk proteins. Acta Biomater 9: 8991-9003, 2013.
15. Wu T, Zhang J, Wang Y, Li D, Sun B, El-Hamshary H, Yin M and Mo X: Fabrication and preliminary study of a biomimetic tri-layer tubular graft based on fibers and fiber yarns for vascular tissue engineering. Mater Sci Eng C Mater Biol Appl 82: 121-129, 2018.
16. Han F, Jia X, Dai D, Yang X, Zhao J, Zhao Y, Fan Y and Yuan X: Performance of a multilayered small-diameter vascular scaffold dual-loaded with VEGF and PDGF. Biomaterials 34: 7302-7313, 2013.
17. de Valence S, Tille JC, Giliberto JP, Mrowczynski W, Gurny R, Walpoth BH and Möller M: Advantages of bilayered vascular grafts for surgical applicability and tissue regeneration. Acta Biomater 8: 3914-3920, 2012.
18. Attalla R, Puersten E, Jain N and Selvaganapathy PR: 3D bioprinting of heterogeneous bi- and tri-layered hollow channels within gel scaffolds using scalable multi-axial microfluidic extrusion nozzle. Biofabrication 11: 015012, 2018.
19. Blakeney BA, Tambralli A, Anderson JM, Andukuri A, Lim DJ, Dean DR and Jun HW: Cell infiltration and growth in a low density, uncompressed three-dimensional electrospun nanofibrous scaffold. Biomaterials 32: 1583-1590, 2011.
20. Wu T, Huang C, Li D, Yin A, Liu W, Wang J, Chen J, Ei-Hamshary H, Al-Deyab SS and Mo X: A multi-layered vascular scaffold with symmetrical structure by bi-directional gradient electrospinning. Colloids Surf B Biointerfaces 133: 179-188, 2015.
21. Garrett IR, Gutierrez G and Mundy GR: Statins and bone formation. Curr Pharm Des 7: 715-736, 2001.
22. Mundy G, Garrett R, Harris S, Chan J, Chen D, Rossini G, Boyce B, Zhao M and Gutierrez G: Stimulation of bone formation in vitro and in rodents by statins. Science 286: 1946-1949, 1999.
23. Thylin MR, McConnell JC, Schmid MJ, Reckling RR, Ojha J, Bhattacharyya I, Marx DB and Reinhardt RA: Effects of simvastatin gels on murine calvarial bone. J Periodontol 73: 1141-1148, 2002.
24. Jiang H, Hu Y, Li Y, Zhao P, Zhu K and Chen W: A facile technique to prepare biodegradable coaxial electrospun nanofibers for controlled release of bioactive agents. J Control Release 108: 237-243, 2005.
25. Zhu H, Yu D, Zhou Y, Wang C, Gao M, Jiang H and Wang H: Biological activity of a nanofibrous barrier membrane containing bone morphogenetic protein formed by core-shell electrospinning as a sustained delivery vehicle. J Biomed Mater Res B Appl Biomater 101: 541-552, 2013.
26. Chen H, Malheiro A, van Blitterswijk C, Mota C, Wieringa PA and Moroni L: Direct writing electrospinning of scaffolds with multidimensional fiber architecture for hierarchical tissue engineering. ACS Appl Mater Interfaces 9: 38187-38200, 2017.
27. Zhang X, Aubin JE and Inman RD: Molecular and cellular biology of new bone formation: Insights into the ankylosis of ankylosing spondylitis. Curr Opin Rheumatol 15: 387-393, 2003.
28. Lee JS, Lee JM and Im GI: Electroporation-mediated transfer of Runx2 and Osterix genes to enhance osteogenesis of adipose stem cells. Biomaterials 32: 760-768, 2011.
29. Wrobel E, Leszczynska J and Brzoska E: The characteristics of human bone-derived cells (HBDCS) during osteogenesis in vitro. Cell Mol Biol Lett 21: 26, 2016.
30. Termine JD, Kleinman HK, Whitson SW, Conn KM, McGarvey ML and Martin GR: Osteonectin, a bone-specific protein linking mineral to collagen. Cell 26: 99-105, 1981.
31. Graneli C, Thorfve A, Ruetschi U, Brisby H, Thomsen P, Lindahl A and Karlsson C: Novel markers of osteogenic and adipogenic differentiation of human bone marrow stromal cells identified using a quantitative proteomics approach. Stem Cell Res 12: 153-165, 2014.
32. Pfaffl MW: A new mathematical model for relative quantification in real-time RT-PCR. Nucleic Acids Res 29: e45, 2001.
33. Bacevic M, Brkovic B, Lambert F, Djukic L, Petrovic N and Roganovic J: Leukocyte- and platelet-rich fibrin as graft material improves microRNA-21 expression and decreases oxidative stress in the calvarial defects of diabetic rabbits. Arch Oral Biol 102: 231-237, 2019.
34. Chen P and Liu B: Study on repair of critical calvarial defects with nano-hydroxyapatite/collagen/polylactic acid material compounded recombinant human bone morphogenetic protein 2 in rabbits. Zhongguo Xiu Fu Chong Jian Wai Ke Za Zhi 21: 1191-1195, 2007 (In Chinese).
35. Durmus E, Celik I, Aydin MF, Yildirim G and Sur E: Evaluation of the biocompatibility and osteoproductive activity of ostrich eggshell powder in experimentally induced calvarial defects in rabbits. J Biomed Mater Res B Appl Biomater 86: 82-89, 2008.
36. Li G, Wang X, Cao J, Ju Z, Ma D, Liu Y and Zhang J: Coculture of peripheral blood CD34+ cell and mesenchymal stem cell sheets increase the formation of bone in calvarial critical-size defects in rabbits. Br J Oral Maxillofac Surg 52: 134-139, 2014.
37. Swain LD, Cornet DA, Manwaring ME, Collins B, Singh VK, Beniker D and Carnes DL: Negative pressure therapy stimulates healing of critical-size calvarial defects in rabbits. Bonekey Rep 2: 299, 2013.
38. Tuusa SM, Peltola MJ, Tirri T, Puska MA, Roytta M, Aho H, Sandholm J, Lassila LVJ and Vallittu PK: Reconstruction of critical size calvarial bone defects in rabbits with glass-fiber-reinforced composite with bioactive glass granule coating. J Biomed Mater Res B Appl Biomater 84: 510-519, 2008.
39. Wang Z, Han L, Sun T, Wang W, Li X and Wu B: Osteogenic and angiogenic lineage differentiated adipose-derived stem cells for bone regeneration of calvarial defects in rabbits. J Biomed Mater Res A 109: 538-550, 2021.
40. Wang Z, Hu H, Li Z, Weng Y, Dai T, Zong C, Liu Y and Liu B: Sheet of osteoblastic cells combined with platelet-rich fibrin improves the formation of bone in critical-size calvarial defects in rabbits. Br J Oral Maxillofac Surg 54: 316-321, 2016.

41. Kammerer PW, Lehnert M, Al-Nawas B, Kumar VV, Hagmann S, Alshihri A, Frerich B and Veith M: Osseoconductivity of a specific streptavidin-biotin-fibronectin surface coating of biotinylated titanium implants-a rabbit animal study. Clin Implant Dent Relat Res 17 (Suppl 2): e601-e612, 2015.
42. Chen Z, Wang L and Jiang H: The effect of procyanidine cross-linking on the properties of the electrospun gelatin membranes. Biofabrication 4: 035007, 2012.
43. Chen Z, Cao L, Wang L, Zhu H and Jiang H: Effect of fiber structure on the properties of the electrospun hybrid membranes composed of poly(ε-caprolactone) and gelatin. J Appl Polymer Sci 127: 4225-4232, 2013.
44. McHugh J: Promising drug delivery system. Nat Rev Rheumatol 15: 64, 2019.
45. Amschler K, Erpenbeck L, Kruss S and Schon MP: Nanoscale integrin ligand patterns determine melanoma cell behavior. ACS Nano 8: 9113-9125, 2014.
46. Qian C, Zhu C, Yu W, Jiang X and Zhang F: High-Fat diet/low-dose streptozotocin-induced type 2 diabetes in rats impacts osteogenesis and wnt signaling in bone marrow stromal cells. PLoS One 10: e0136390, 2015.
47. Seif S, Planz V and Windbergs M: Delivery of therapeutic proteins using electrospun fibers-recent developments and current challenges. Arch Pharm (Weinheim) 350: 1700077, 2017.
48. Yin L, Wang K, Lv X, Sun R, Yang S, Yang Y, Liu Y, Liu J, Zhou J and Yu Z: The fabrication of an ICA-SF/PLCL nanofibrous membrane by coaxial electrospinning and its effect on bone regeneration in vitro and in vivo. Sci Rep 7: 8616, 2017.
49. Bigi A, Cojazzi G, Panzavolta S, Rubini K and Roveri N: Mechanical and thermal properties of gelatin films at different degrees of glutaraldehyde crosslinking. Biomaterials 22: 763-768, 2001.
50. Yi H, Ur Rehman F, Zhao C, Liu B and He N: Recent advances in nano scaffolds for bone repair. Bone Res 4: 16050, 2016.
51. Gilbert TW, Stewart-Akers AM and Badylak SF: A quantitative method for evaluating the degradation of biologic scaffold materials. Biomaterials 28: 147-150, 2007.
52. Sung HJ, Meredith C, Johnson C and Galis ZS: The effect of scaffold degradation rate on three-dimensional cell growth and angiogenesis. Biomaterials 25: 5735-5742, 2004.
53. Alsberg E, Kong HJ, Hirano Y, Smith MK, Albeiruti A and Mooney DJ: Regulating bone formation via controlled scaffold degradation. J Dent Res 82: 903-908, 2003.
54. Zhang B, Zhang PB, Wang ZL, Lyu ZW and Wu H: Tissue-engineered composite scaffold of poly(lactide-co-glycolide) and hydroxyapatite nanoparticles seeded with autologous mesenchymal stem cells for bone regeneration. J Zhejiang Univ Sci B 18: 963-976, 2017.
55. Gong YY, Xue JX, Zhang WJ, Zhou GD, Liu W and Cao Y: A sandwich model for engineering cartilage with acellular cartilage sheets and chondrocytes. Biomaterials 32: 2265-2273, 2011.
56. Yin L, Yang S, He M, Chang Y, Wang K, Zhu Y, Liu Y, Chang Y and Yu Z: Physicochemical and biological characteristics of BMP-2/IGF-1-loaded three-dimensional coaxial electrospun fibrous membranes for bone defect repair. J Mater Sci Mater Med 28: 94, 2017.
57. Mi R, Liu Y, Chen X and Shao Z: Structure and properties of various hybrids fabricated by silk nanofibrils and nanohydroxyapatite. Nanoscale 8: 20096-20102, 2016.
58. Teo BK, Wong ST, Lim CK, Kung TY, Yap CH, Ramagopal Y, Romer LH and Yim EKF: Nanotopography modulates mechanotransduction of stem cells and induces differentiation through focal adhesion kinase. ACS Nano 7: 4785-4798, 2013.
59. Stein D, Lee Y, Schmid MJ, Killpack B, Genrich MA, Narayana N, Marx DB, Cullen DM and Reinhardt RA: Local simvastatin effects on mandibular bone growth and inflammation. J Periodontol 76: 1861-1870, 2005.
60. Khan H, Mafi P, Mafi R and Khan W: The effects of ageing on differentiation and characterisation of human mesenchymal stem cells. Curr Stem Cell Res Ther 13: 378-383, 2018.
61. Prall WC, Saller MM, Scheumaier A, Tucholski T, Taha S, Bocker W and Polzer H: Proliferative and osteogenic differentiation capacity of mesenchymal stromal cells: Influence of harvesting site and donor age. Injury 49: 1504-1512, 2018.
62. Mendes SC, Tibbe JM, Veenhof M, Bakker K, Both S, Platenburg PP, Oner FC, de Bruijn JD and van Blitterswijk CA: Bone tissue-engineered implants using human bone marrow stromal cells: Effect of culture conditions and donor age. Tissue Eng 8: 911-920, 2002.
63. Hu ML: Osteogenic differentiation ability and related gene profiles of bone marrow mesenchymal stem cells derived from different ages (unpublished PhD thesis). Tianjin Medical University, 2019.
64. Choudhery MS, Khan M, Mahmood R, Mehmood A, Khan SN and Riazuddin S: Bone marrow derived mesenchymal stem cells from aged mice have reduced wound healing, angiogenesis, proliferation and anti-apoptosis capabilities. Cell Biol Int 36: 747-753, 2012.
65. Fossett E, Khan WS, Pastides P and Adesida AB: The effects of ageing on proliferation potential, differentiation potential and cell surface characterisation of human mesenchymal stem cells. Curr Stem Cell Res Ther 7: 282-286, 2012.
66. Stolzing A, Jones E, McGonagle D and Scutt A: Age-related changes in human bone marrow-derived mesenchymal stem cells: Consequences for cell therapies. Mech Ageing Dev 129: 163-173, 2008.
67. Aksoy C, Kaya FA, Kuskonmaz BB, Uckan D and Severcan F: Structural investigation of donor age effect on human bone marrow mesenchymal stem cells: FTIR spectroscopy and imaging. Age (Dordr) 36: 9691, 2014.